## **Inorganic Chemistry**

pubs.acs.org/IC Article

# Molecular Flexibility in Solvated Crystals of the Dimer, $Au_2(\mu-1,2-bis(diphenylphosphino)ethane)_2l_2$ , with Three-Coordinate Gold(I)

Sarah Costa, Michael M. Aristov, Sang Ho Lim, Sarah M. Chui, Katelyn A. Espinoza, Marilyn M. Olmstead, James C. Fettinger, John F. Berry,\* and Alan L. Balch\*

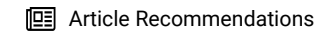


Cite This: Inorg. Chem. 2024, 63, 12752–12763



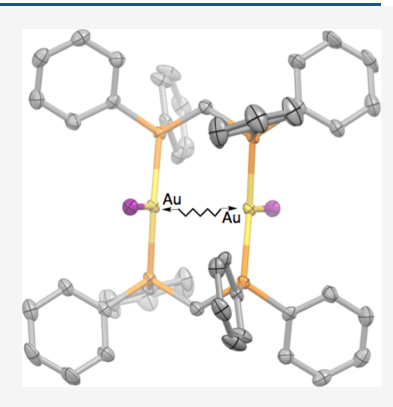
**ACCESS** |

III Metrics & More



Supporting Information

**ABSTRACT:** We report the ability to trap the dimer  $Au_2(\mu\text{-dppe})_2I_2$  (dppe is 1,2-bis(diphenylphosphino)ethane) with different separations between the three-coordinate gold ions in crystalline solvates. All of these solvates ( $(Au_2(\mu\text{-dppe})_2I_2\cdot 4(CH_2Cl_2)$  (1),  $Au_2(\mu\text{-dppe})_2I_2\cdot 2(CH_2Cl_2)$  (2), the polymorphs α- $Au_2(\mu\text{-dppe})_2I_2\cdot 2(HC(O)NMe_2)$  (3) and β- $Au_2(\mu\text{-dppe})_2I_2\cdot 2(HC(O)NMe_2)$  (4), and  $Au_2(\mu\text{-dppe})_2I_2\cdot 4(CHCl_3)$  (5)) along with polymeric { $Au(\mu\text{-dppe})I\}_n\cdot n(CHCl_3)$  (6)) originated from the same reaction, only the solvent system used for crystallization differed. In the different solvates of  $Au_2(\mu\text{-dppe})_2I_2$ , the  $Au\cdots Au$  separation varied from 3.192(1) to 3.7866(3) Å. Computational studies undertaken to understand the flexible nature of these dimers indicated that the structural differences were primarily a result of crystal packing effects with aurophillic interactions having a minimal effect.



## **■ INTRODUCTION**

Diphosphine ligands have been used to prepare a range of binuclear, polynuclear, and polymeric metal complexes. <sup>1,2</sup> In particular, ligands of the type  $R_2P(CH_2)_nPR_2$  have been used to form binuclear, macrocyclic complexes with an  $M_2(\mu-R_2P-(CH_2)_nR_2)_2$  core with varying distances between the metal ions. When n is 1, the ligand places the metal centers in close proximity and facilitates bonding between these metal centers. <sup>3,4</sup> When n is three or more, the metal centers are generally widely separated and not directly interacting with one another. <sup>5-11</sup> However, when n is 2, the bridging ligand can accommodate a range of separations between the metal centers. <sup>9,12,13</sup>

The remarkable flexibility of the bridging diphosphine ligand 1,2- bis(diphenyl)phosphinoethane (dppe) in the dimers  $Au_2(\mu\text{-dppe})_2I_2$  and  $Au_2(\mu\text{-dppe})_2Br_2$  produced solvated crystals with varying Au···Au separations and some unusual luminescence properties. 12,13 Scheme 1 shows the behavior of crystals containing the dimer Au<sub>2</sub>( $\mu$ -dppe)<sub>2</sub>I<sub>2</sub> and related compounds.<sup>13</sup> The two polymorphs of the acetone solvate  $Au_2(\mu\text{-dppe})_2I_2\cdot 2(OCMe_2)$  exhibit different luminescence and different separations between the planar, three-coordinate gold ions. Upon brief exposure to air, the orange luminescent  $\alpha$ polymorph with an Au···Au distance of 3.6720(2) Å was converted into the green luminescent  $\beta$ -polymorph with an Au··· Au distance of 3.3955(3) Å. This process could be reversed by exposure of the crystals to acetone vapor. However, upon prolonged standing in air, the  $\beta$ -polymorph lost acetone to form a green luminescent powder that was converted into orange luminescent  $Au_2(\mu$ -dppe)<sub>2</sub>( $\mu$ -I)<sub>2</sub> upon exposure to acetone vapor. Crystals containing the dimer  $Au_2(\mu$ -dppe)<sub>2</sub>Br<sub>2</sub> also

displayed a range of Au···Au distances that extended from 3.0943(2) to 3.8479(3) Å and displayed varying luminescence: green when the Au···Au distance was less than 3.5 Å, orange when it was greater than 3.5 Å. Even shorter Au···Au distances (in the range 2.8787(9) to 2.9593(5) Å) occur in the cationic dimers,  $\left[\mathrm{Au}_2(\mu\text{-dppe})_2\right]^{2+}$ , which involve two-coordinate, rather than three-coordinate gold(I) ions.  $^{11,14}$ 

The variation in the Au···Au distances in the solvates of  $Au_2(\mu\text{-dppe})_2I_2$  and  $Au_2(\mu\text{-dppe})_2Br_2$  suggested that aurophilic interactions between the two gold ions might influence the structure and luminescence of the crystals. Aurophilic interactions between closed-shell  $d^{10}$  Au(I) ions occur when there are short distances between adjacent gold(I) ions and involve mixing of the filled 5d orbitals with the empty 6s and 6p gold orbitals. Such interactions are particularly prevalent in two-coordinate gold(I) complexes and are likely to occur when the Au···Au separation is shorter than the distance of about 3.6 Å expected from simple van der Waals factors.

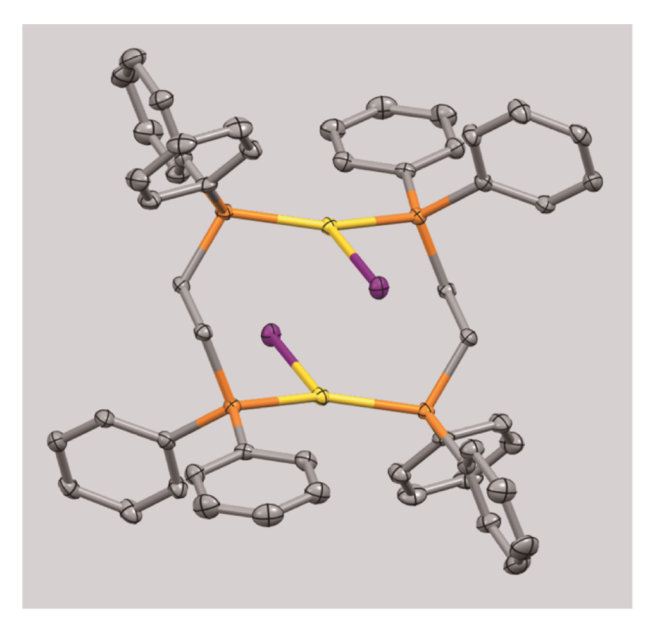
Here, we report the structures and luminescent behavior of new crystalline solvates of  $Au_2(\mu\text{-dppe})_2I_2$  along with computational studies designed to understand the factors responsible for the variations in Au···Au distances in these crystals.

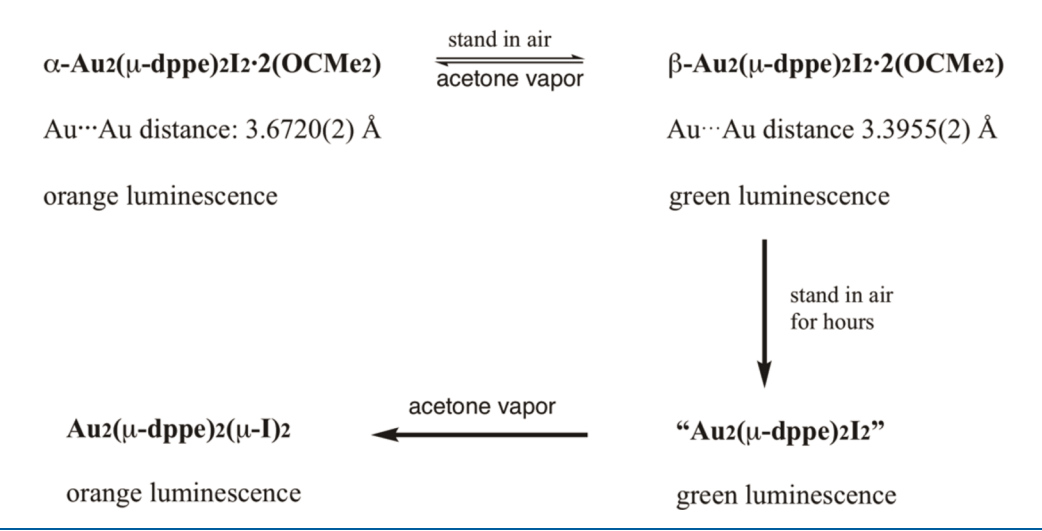
Received: February 25, 2024 Revised: June 10, 2024 Accepted: June 19, 2024 Published: July 2, 2024





Scheme 1. Crystal Transformations of the Polymorphs of  $Au_2(\mu\text{-dppe})_2I_2\cdot 2(OCMe_2)$  and Related Compounds from Data in Ref 13





#### RESULTS AND DISCUSSION

Preparation and Crystal Growth. Addition of dppe to a slurry of solid AuI in acetone or dichloromethane produced a colorless solution, which yielded a colorless solid upon evaporation. This colorless solid was crystallized from three different solvents to yield pairs of crystalline compounds as outlined below. Crystal data for the six compounds are set out in Table 1. Significant interatomic distances and angles are given in Table 2.

Crystallization from Dichloromethane: Formation of Solvates  $Au_2(\mu\text{-dppe})_2I_2\cdot 4(CH_2CI_2)$  (1) and  $Au_2(\mu\text{-dppe})_2I_2\cdot 2(CH_2CI_2)$  (2). Crystals of the two solvates,  $Au_2(\mu\text{-dppe})_2I_2\cdot 4(CH_2CI_2)$  (1) and  $Au_2(\mu\text{-dppe})_2I_2\cdot 2(CH_2CI_2)$  (2), were obtained individually by diffusion of diethyl ether into a dichloromethane solution of the colorless solid mentioned above. Oddly, the sample of  $Au_2(\mu\text{-dppe})_2I_2\cdot 4(CH_2CI_2)$  (1) was obtained during the summer, while sample of  $Au_2(\mu\text{-dppe})_2I_2\cdot 2(CH_2CI_2)$  (2) was obtained during the winter. Based on their luminescence and crystal morphology, each of the samples appeared to be homogeneous. The structure of  $Au_2(\mu\text{-dppe})_2I_2\cdot 4(LH_2CI_2)$  (2) was obtained our morphology.

 $4(CH_2Cl_2)$  (1) is shown in Figure 1. The asymmetric unit of the gold complex consists of a gold ion, an iodide ion, and a bridging dppe ligand with the rest of the molecule created by reflection through a center of symmetry. The distance between the two gold ions is 3.192(1) Å, which is the shortest such distance in the complexes reported here. Each gold ion exhibits planar, three-coordinate geometry. The P–Au–P angle is much wider than the two P–Au–I angles, but the sum of the three angles is close to  $360^{\circ}$ . This situation is characteristic of other molecules with two phosphine ligands and an iodide ligand as can be seen in Table 3. The four solvate molecules are rather far from the gold ions. The closest interaction is the 5.473 Å distance between a gold ion and a hydrogen atom of the nearest dichloromethane molecule.

The structure of  $\text{Au}_2(\mu\text{-dppe})_2\text{I}_2\cdot 2(\text{CH}_2\text{Cl}_2)$  (2) is similar to that of  $\text{Au}_2(\mu\text{-dppe})_2\text{I}_2\cdot 4(\text{CH}_2\text{Cl}_2)$  (1). In both solvates, the dimeric complexes are centrosymmetric. However, the separation between the two gold ions is longer in  $\text{Au}_2(\mu\text{-dppe})_2\text{I}_2\cdot 2(\text{CH}_2\text{Cl}_2)$  (2) (3.5013(2) Å) than in  $\text{Au}_2(\mu\text{-dppe})_2\text{I}_2\cdot 4(\text{CH}_2\text{Cl}_2)$  (1) (3.192(1) Å). Additionally, the distance

Table 1. Crystal Data and Data Collection Parameters

	$Au2(\mu-dppe)2I2·4(CH2Cl2) (1)$	$Au2(\mu-dppe)2I2·2(CH2Cl2) (2)$	$\alpha$ -Au <sub>2</sub> ( $\mu$ -dppe) <sub>2</sub> I <sub>2</sub> ·2(HC(O)NMe <sub>2</sub> ) (3
formula	$C_{56}H_{56}Au_2Cl_8I_2P_4$	$C_{54}H_{52}Au_2Cl_4I_2P_4$	$C_{58}H_{62}Au_2I_2NOP_4$
formula weight	1784.22	1614.37	1590.72
Т, К	100.15	100(2)	90(2) K
color and habit	colorless block	colorless block	colorless plate
crystal system	monoclinic	monoclinic	triclinic
space group	$P2_1/c$	$P2_1/c$	$P\overline{1}$
a, Å	13.539(4)	10.7304(4)	11.9418(5)
b, Å	22.002(7)	22.6930(8)	12.0967(5)
e, Å	10.801(4)	11.9931(4)	12.5362(5)
α, deg	90	90	63.892(2)
β, deg	110.057(14)	108.4470(10)	68.434(2)
γ, deg	90	90	64.039(2)
V, Å <sup>3</sup>	3022.3(17)	2770.32(17)	1427.31(10)
Z	2	4	1
d <sub>calcd</sub> , g·cm <sup>-3</sup>	1.961	3.148	1.816
u, mm <sup>-1</sup>	6.366	13.268	6.366
unique data	6960	6370	6513
restraints	0	0	0
parameters.	325	309	318
R <sub>1</sub> <sup>a</sup>	0.0404	0.0267	0.0163
$wR_2^b$	0.1001	0.0602	0.0500
	$\beta$ -Au <sub>2</sub> ( $\mu$ -dppe) <sub>2</sub> I <sub>2</sub> ·2(HC(O)NMe <sub>2</sub> )	(4) $\text{Au}_2(\mu\text{-dppe})_2\text{I}_2 \cdot 4(\text{CHCl}_3)$ (5)	${Au(\mu\text{-dppe})I}_n \cdot n(CHCl_3)$ (
formula	$C_{58}H_{62}Au_2I_2N_2O_2P_4$	$C_{56}H_{52}Au_2Cl_{12}I_2P_4$	$C_{27}H_{25}AuCl_3IP_2$
formula weight	1590.71	1921.99	841.63
T, K	90(2) K	100(2)	90(2) K
color and habit	colorless plate	colorless block	colorless irregular plate
crystal system	triclinic	triclinic	triclinic
space group	$P\overline{1}$	$P\overline{1}$	$P\overline{1}$
a, Å	11.9340(5)	10.5616(11)	10.0425(7)
b, Å	14.2277(6)	12.7861(13)	11.4032(8)
c, Å	18.4006(8)	13.0433(14)	13.7462(10)
α, deg	83.4850(10)	69.469(2)	76.248(10)
β, deg	89.3280(10)	83.592(2)	88.288(1)
γ, deg	66.3480(10)	88.929(2)	70.641(1)
V, Å <sup>3</sup>	2841.4(2)	1638.8(3)	1440.53(18)
Z	2	1	2
d <sub>calcd</sub> , g⋅cm <sup>-3</sup>	1.859	1.947	1.939
<i>u</i> , mm <sup>-1</sup>	6.399	6.036	6.578
unique data	13954	9479	6582
restraints	0	0	0
parameters	635	344	307
$R_1^a$	0.0399	0.0178	0.0411
K1			0.01.1

between the two phosphorus atoms in the bridging dppe ligand is longer in  $Au_2(\mu\text{-dppe})_2I_2\cdot 2(CH_2Cl_2)$  (2) (4.116(1) Å) than in  $Au_2(\mu\text{-dppe})_2I_2\cdot 4(CH_2Cl_2)$  (1) (4.025(2) Å).

Colorless crystals of  $Au_2(\mu\text{-dppe})_2I_2\cdot 4(CH_2Cl_2)$  (1) and  $Au_2(\mu\text{-dppe})_2I_2\cdot 2(CH_2Cl_2)$  (2) are photoluminescent. Figure 2 shows the excitation and emission spectra for the two complexes at room temperature and at 77 K. These spectra and all other excitation and emission spectra reported here were obtained from crystalline samples that were handled to minimize the loss of solvate molecules, which could result in alteration of the spectroscopic properties as has been reported previously. Information about the excitation and emission maxima for these and other crystals are shown in Table 4. At room temperature, both complexes show a single excitation band at 378–384 nm

and a single emission band at 556 nm for compound (1) or 594 nm for compound (2). At 77 K, the emission bands shift to longer wavelengths without a significant change in the excitation spectrum. For  $\text{Au}_2(\mu\text{-dppe})_2\text{I}_2\cdot2(\text{CH}_2\text{Cl}_2)$  (2), the emission lifetime at room temperature is 9  $\mu$ s, while at 77 K, it lengthens to 14  $\mu$ s. These lifetimes suggest that the emission arises from phosphorescence.

Polymorphs of Au<sub>2</sub>( $\mu$ -dppe)<sub>2</sub>l<sub>2</sub>·2(HC(O)NMe<sub>2</sub>). Evaporation of an *N*,*N*-dimethylformamide solution of the colorless complex obtained from adding dppe to AuI in dichloromethane produced colorless crystals of the  $\alpha$ -polymorph, which displayed a yellow-green luminescence along with colorless crystals of the  $\beta$ -polymorph that produced yellow emission. Figure 3 shows photographs of crystals of both  $\alpha$ -Au<sub>2</sub>( $\mu$ -dppe)<sub>2</sub>I<sub>2</sub>·2(HC(O)-

Table 2. Selected Interatomic Distances (Å) and Angles (deg) for Gold Complexes

distances (A	Au <sub>2</sub> ( $\mu$ -dppe) <sub>2</sub> I <sub>2</sub> ·4(CH <sub>2</sub> Cl <sub>2</sub>	$Au_2(\mu\text{-dppe})_2I_2\cdot 2(CH_2CI_2)$	2) (2) α-Au <sub>2</sub> (μ-dpp	$\alpha$ -Au <sub>2</sub> ( $\mu$ -dppe) <sub>2</sub> I <sub>2</sub> ·2(HC(O)NMe <sub>2</sub> ) (3)	
Au1···Au1A	3.192(1)	3.5013(2)		3.4289(2)	
P1…P2	4.025(2)	4.116(1)		4.0888(9)	
Au1-I1	2.9173(9)	2.9045(3)		2.9699(2)	
Au1-P1	2.315(2)	2.3182(9)		2.3170(7)	
Au1-P2	2.326(2)	2.3126(8)		2.3156(8)	
angles (deg)					
P1···Au1···P2	148.24(6)	153.24(3)		152.91(2)	
P1···Au1···I1	108.56(4)	103.40(2)		103.07(2)	
P2···Au1···I1	102.65(4)	102.94(2)	103.55(2)		
$\Sigma$ angles about	: Au1 359.45	359.58		359.53	
distances (Å)	β-Au <sub>2</sub> ( $μ$ -dppe) <sub>2</sub> I <sub>2</sub> ·2(HC(O)NMe <sub>2</sub> ) (4) site A	$\beta$ -Au <sub>2</sub> ( $\mu$ -dppe) <sub>2</sub> I <sub>2</sub> ·2(HC(O)NMe <sub>2</sub> ) (4) site B	$\begin{array}{c} \operatorname{Au}_{2}(\mu\text{-dppe})_{2}\operatorname{I}_{2}\cdot 4(\operatorname{CHCl}_{3}) \\ (5) \end{array}$	$ {Au(\mu\text{-dppe})I}_n \cdot n(CHCl_3)  (6) $	
Au1···Au1A	3.2366(3)	3.7866(3)	3.5959(5)	7.1910(7)	
P1P2	4.040(2)	4.202(2)	4.1251(8)	4.437(2)	
Au1-I1	3.0044(4)	3.0055(4)	2.9296(4)	2.8499(4)	
Au1-P1	2.301(2)	2.320(2)	2.3183(7)	2.316(2)	
Au1-P2	2.310(2)	2.318(2)	2.3162(7)	2.300(2)	
angles (deg)					
P1···Au1···P2	155.43(6)	160.12(6)	153.92(2)	148.03(6)	
P1···Au1···I1	102.52(4)	100.44(4)	102.45(2)	101.98(4)	
P2···Au1···I1	99.22(4)	99.40(4)	103.45(2)	108.43(4)	
$\Sigma$ angles about Au1	357.17	359.96	359.82	358.44	

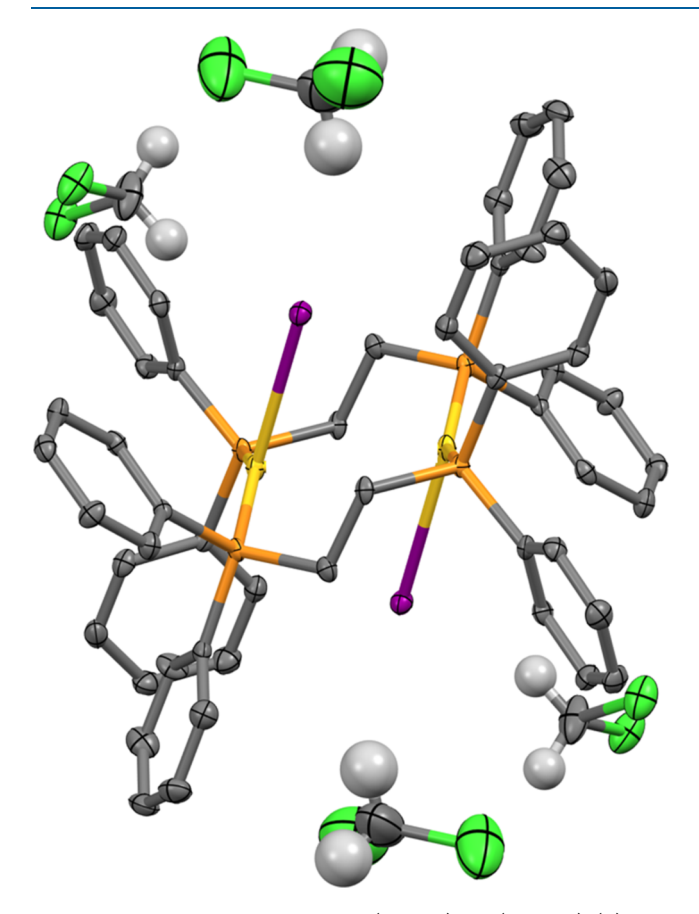


Figure 1. Molecular structure of  $Au_2(\mu$ -dppe) $_2I_2$ ·4( $CH_2CI_2$ ) (1) with the hydrogen atoms removed for clarity except for those on the dichloromethane molecules. Color code: gold, yellow; phosphorus, orange; iodine, purple; carbon, gray; chlorine, green; hydrogen, white.

NMe<sub>2</sub>) (3) and  $\beta$ -Au<sub>2</sub>( $\mu$ -dppe)<sub>2</sub>I<sub>2</sub>·2(HC(O)NMe<sub>2</sub>) (4) under ambient and ultraviolet (UV) light. The crystals were separated

manually based on their morphology and luminescence to provide samples for spectroscopic investigation. The excitation and emission maxima for the two different polymorphs are given in Table 4.

Crystals of  $\alpha$ -Au<sub>2</sub>( $\mu$ -dppe)<sub>2</sub>I<sub>2</sub>·2(HC(O)NMe<sub>2</sub>) (3) contain a centrosymmetric Au<sub>2</sub>( $\mu$ -dppe)<sub>2</sub>I<sub>2</sub> molecule, whose structure is similar to the dimers in crystals of (1) and (2). In  $\alpha$ -Au<sub>2</sub>( $\mu$ -dppe)<sub>2</sub>I<sub>2</sub>·2(HC(O)NMe<sub>2</sub>) (3), the separation between the two gold ions is 3.4289(2) Å. The other dimensions of this dimer are given in Table 2.

The  $\beta$ -polymorph contains two distinct centrosymmetric dimers with different distances between the gold ions: 3.7866(3)and 3.2366(3) Å. One of the dimers in this polymorph contains the longest Au···Au separation seen in this study. The structures of the two different dimers are compared in Figure 4. In addition to the variation in Au···Au distances, the orientations of the phenyl rings are different in the two molecules. In the molecule with the shorter separation between the gold ions, the two phenyl rings that protrude toward the viewer in Figure 4 are roughly perpendicular to one another, and the two phenyl rings that extend away from the viewer at the back of the dimer are also roughly perpendicular to one another. In contrast, in the molecule with the longer separation between the gold ions seen at the bottom of Figure 4, the two phenyl rings that protrude toward the viewer are roughly parallel to one another as are the two phenyl rings that extend away for the viewer on the back side of the molecule.

Crystallization from Chloroform: Formation of Dimeric  $Au_2(\mu\text{-}dppe)_2l_2\cdot 4(CHCl_3)$  (5) and Polymeric  $\{Au(\mu\text{-}dppe)\}l_n\cdot n(CHCl_3)$  (6). Layering diethyl ether over a chloroform solution of the product from the reaction between gold(I) iodide and dppe produced colorless blocks of  $Au_2(\mu\text{-}dppe)_2I_2\cdot 4(CHCl_3)$  (5), which displayed green luminescence under UV irradiation. Excitation and emission data are given in Table 4. The structure of the complex is similar to the other gold dimers reported here. The separation between the gold ions is 3.5959(5) Å.

Table 3. Selected Bond Distances (Å) and Angles (deg) for Three-Coordinate Gold Complexes<sup>d</sup>

	. ,		-	
	$Au(PCy_3)_2I^a$	$Au(PCy_3)_2I\cdot PCy_3^a$	$Au(PPh_3)_2I^b$	$Au_2(\mu$ -dcmp $)_2I_2^c$
bond angles (Å)				
Au1-I1	2.895(2)	3.008(1)	2.7588(6)	2.9960(7)
Au1-P1	2.344(2)	2.315(3)	2.3331(1)	2.342(3)
Au1-P2	2.328(2)	2.310(3)	2.3331(1)	2.321(3)
Au···Au				3.0756(6)
bond angles (deg)				
P1···Au1···P2	143.1(1)	159.1(1)	131.86(6)	157.93(7)
P1···Au1···I1	106.26(7)	98.69(7)	114.07(3)	94.40(6)
P2···Au1···Br1	110.45(7)	101.87(7)	114.07(3)	107.62(6)
$\Sigma$ angles about Au1	359.81	359.66	360.00	359.95
	$[\{Au_2(\mu\text{-dmpe})_2\}_2\mu\text{-I}]^a$ Au1	$[\{Au_2(\mu\text{-dmpe})_2\}_2\mu\text{-I}]^a Au2$	$[{Au_2(\mu\text{-dmpe})_2}_2\mu\text{-I}]^a$ Au3	$[{Au2(\mu\text{-dmpe})2}2\mu\text{-I}]^a$ Au4
bond distances (Å)				
Au1-I1	3.267(2)	3.331(2)	3.151(2)	3.277(2)
Au1-P1	2.287(5)	2.285(5)	2.292(5)	2.297(2)
Au1-P2	2.294(5)	2.287(5)	2.291(5)	2.310(5)
Au···Au	2.971(2)	2.971(2)	2.976(1)	2.976(1)
bond angles (deg)				
P1-Au1-P2	174.0(2)	176.0(2)	171.6(2)	178.6(2)
P1-Au1-I1	93.8(1)	87.8(1)	89.6(1)	93.8(1)
P2-Au1-I1	89.4(1)	89.2(1)	94.3(1)	84.8(1)
$\Sigma$ angles about Au1	357.2	353.0	355.5	357.2
	$[Au_3(\mu\text{-dpmp})_2 (\mu\text{-I})]$	]I <sup>e</sup> Au1 [Au <sub>3</sub> ( $\mu$ -dpr	$mp)_2 (\mu-I)I]I^e Au2$	$[Au_3(\mu\text{-dpmp})_2 (\mu\text{-I})I]I^e$ Au3
bond distances (Å)				
Au1-I1	3.008(1)	3	.036(1)	3.191(1)
Au1-P1	2.306(3)	2	.309(3)	2.313(3)
Au1-P2	2.316(3)	2	.321(3)	2.315(3)
Au···Au	2.9525(9)	2	.9525(9)	3.0202(9)
		3	.0202(9)	
bond angles (deg)				
P1-Au1-P2	173.0(1)	1	55.3(1)	170.4(1)
P1-Au1-I1	93.37(8)	1	03.46(8)	95.89(8)
P2-Au1-I1	93.44(8)	1	01.15(8)	91.42(8)
$\Sigma$ angles about Au1	359.81	3	59.91	357.71

"Data from PCy<sub>3</sub> = tricyclohexylphosphine. Bowmaker, G. A.; Brown, C. L.; Hart, R. D.; Healy, P. C.; Englehardt, L. M.; Rickard, C. E. F.; White, A. H. *J. Chem. Soc. Dalton Trans.* **1999**, 881–889. <sup>b</sup>Fränkel, R.; Kniczek, J.; Ponikwar, W.; Nöth, H.; Polborn, K.; Fehlhammer, W. P. *Inorg. Chim. Acta* **2001**, 312, 23. 'dcmp = bis(dicyclohexylphosphino)methane, centrosymmetric dimer. Fu. W.-F.; Chan, K.-C.; Cheung, K.-K.; Che, C.-M. *Chem. Eur. J.* **2001**, 7, 4656. <sup>d</sup>dmpe = bis(dimethylphosphino)ethane. Jaw, H.-R. C.; Savas, M. M.; Rogers, R. D.; Mason, W. R. *Inorg. Chem.* **1989**, 28, 1028–1037. <sup>e</sup>dpmp = bis(diphenylphosphinomethyl)phenylphosphine. Xiao, H.; Weng, Y.-X. Wong, W.-T.; Mak, T. C. W.; Che, C.-M. *Dalton Trans.*, **1997**, 221–226.

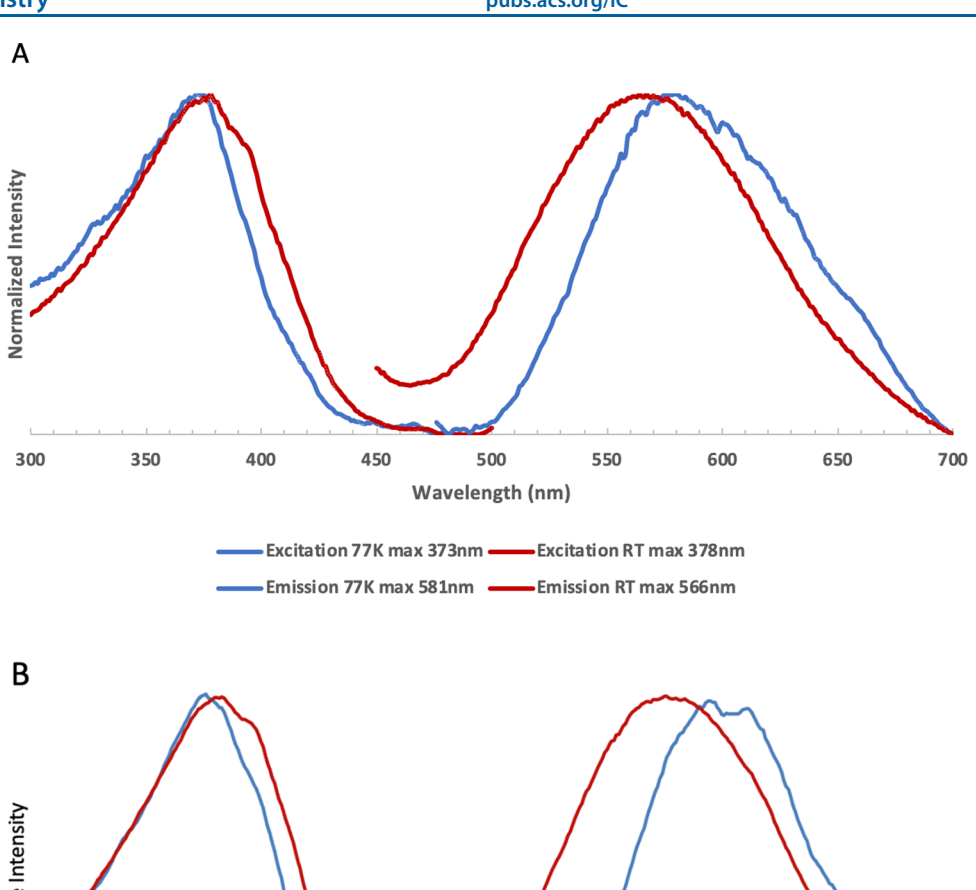
Colorless blocks of the polymer  $\{Au(\mu\text{-dppe})I\}_n \cdot n(CHCl_3)$ (6) were obtained by layering pentane over a chloroform solution of the initial colorless product. A portion of the structure of the product is shown in Figure 5. The asymmetric unit consists of a chloroform molecule in a general position and a CH<sub>2</sub>Ph<sub>2</sub>PAuIPPh<sub>2</sub>CH<sub>2</sub> unit with the rest of each dppe ligand formed by reflection through a center of inversion. Within the polymer, the gold center is planar and coordinated to a terminal iodide ligand and phosphorus atoms from two different bridging ligands. The gold ions are widely separated in these polymers. The closest contact between two gold centers is 6.7401(7) Å within a chain and 10.0425(7) Å between different chains. Clearly, there are no aurophilic interactions in these polymers. The structure of polymeric  $\{Au(\mu\text{-dppe})I\}_n \cdot n(CHCl_3)$  (6) is similar to the structures of  $\{Au(\mu\text{-dppe})Br\}_n \cdot (CH_2Cl_2)$  and  ${Au(\mu\text{-dppe})Br}_n \cdot 0.5(C_4H_{10}O)$  reported previously, <sup>12</sup> but none of these crystals are isostructural.

The polymer is not luminescent at room temperature but becomes luminescent ( $\lambda_{\rm max}$  for excitation, 300, 347 nm;  $\lambda_{\rm max}$  for emission 437 nm) when cooled to 77 K. The lack of

luminescence at room temperature is somewhat unusual, particularly since the related polymers,  $\{Au(\mu\text{-dppe})Br\}_n\cdot(CH_2Cl_2)$  and  $\{Au(\mu\text{-dppe})Br\}_n\cdot0.5(C_4H_{10}O)$ , are luminescent at room temperature as are many other three-coordinate gold(I) complexes.  $^{7,12}$ 

Computational Analysis of Structural Differences. Computational methods were employed to better understand the energetics and the nature of the Au···Au interactions in structures of dimeric  $\operatorname{Au}_2(\mu\text{-dppe})_2\operatorname{I}_2$ . Au····Au distances in this family of compounds span an unusually large range, from 3.19 to 3.79 Å. In order to probe the factors controlling this distance, we have performed computational analysis on two structures that correspond to the two polymorphs of previously reported  $\operatorname{Au}_2(\mu\text{-dppe})_2\operatorname{I}_2\cdot 2(\operatorname{OC}(\operatorname{CH}_3)_2):^{13}\operatorname{Geom}(\operatorname{Short})$  with an Au····Au distance of 3.3177(7) Å and  $\operatorname{Geom}(\operatorname{Long})$  with an Au····Au distance of 3.6720(2) Å.

Geometry optimizations starting from crystallographic coordinates were used to locate energetic minima corresponding to these structures. To optimize geometries for these two structures, the Au···Au distances were constrained while all



300 350 400 450 500 550 600 650 700

Wavelength(nm)

— Excitation 77K max 372nm — Excitation RT max 384nm
— Emission 77K max 598nm — Emission RT max 594nm

Figure 2. Excitation and emission spectra from crystalline solids of (A) Au<sub>2</sub>( $\mu$ -dppe)<sub>2</sub>I<sub>2</sub>·4(CH<sub>2</sub>Cl<sub>2</sub>) and (B) Au<sub>2</sub>( $\mu$ -dppe)<sub>2</sub>I<sub>2</sub>·2(CH<sub>2</sub>Cl<sub>2</sub>) (2).

Table 4. Excitation and Emission Spectral Data

compound	temp. (K)	excitation (nm)	emission (nm)
$Au_2(\mu\text{-dppe})_2I_2\cdot 4(CH_2Cl_2)$ (1)	298	378	556
	77	373	581
$Au_2(\mu\text{-dppe})_2I_2\cdot 2(CH_2Cl_2)$ (2)	298	384	594
	77	372	598
$\alpha$ -Au <sub>2</sub> ( $\mu$ -dppe) <sub>2</sub> I <sub>2</sub> ·2(HC(O)NMe <sub>2</sub> ) (3)	298	371	581
$\beta$ -Au <sub>2</sub> ( $\mu$ -dppe) <sub>2</sub> I <sub>2</sub> ·2(HC(O)NMe <sub>2</sub> )	298	394	570
(4)	77	378	572
$Au_2(\mu\text{-dppe})_2I_2\cdot 4(CHCl_3)$ (5)	298	365	537
	77	395	540
${Au(\mu\text{-dppe})I}_n \cdot n(CHCl_3)$ (6)	298	none	none
	77	300, 347	437

other distances were allowed to optimize. A third hypothetical structure, **Geom(Very\_Short)**, with an Au—Au distance of 2.987 Å, well below the sum of the Au van der Waals radii, was

obtained from a full geometry optimization (including the Au---Au distance) starting from the **Geom(Short)** structure. Selected measurements and comparisons between the computational structures and their experimental counterparts are noted in Table 5. A notable difference between Geom(Short) and **Geom**(Long) is the Au···I interaction between the gold center and the iodine atom bound to the other gold center. As the Au··· Au distance shrinks, so does this Au…I interaction, and in the **Geom(Very Short)**, this distance is smaller than the sum of the van der Waals radii, 3.64 Å. No significant differences in other noncovalent interactions were observed between the three optimized structures. Frequency calculations confirm that all three structures occupy local energetic minima, and allow comparison of the Gibbs free energies,  $\Delta G$ , of the structures. **Geom(Very\_Short)** was found to be lowest in  $\Delta G$  (at 298.15 K), followed by Geom(Short) (+9.2 kJ mol<sup>-1</sup>), followed by Geom(Long) (+18.4 kJ mol<sup>-1</sup>). The change in calculated energy between the short and long structures (<10 kJ/mol) is within the associated range of crystal packing effects, which, for

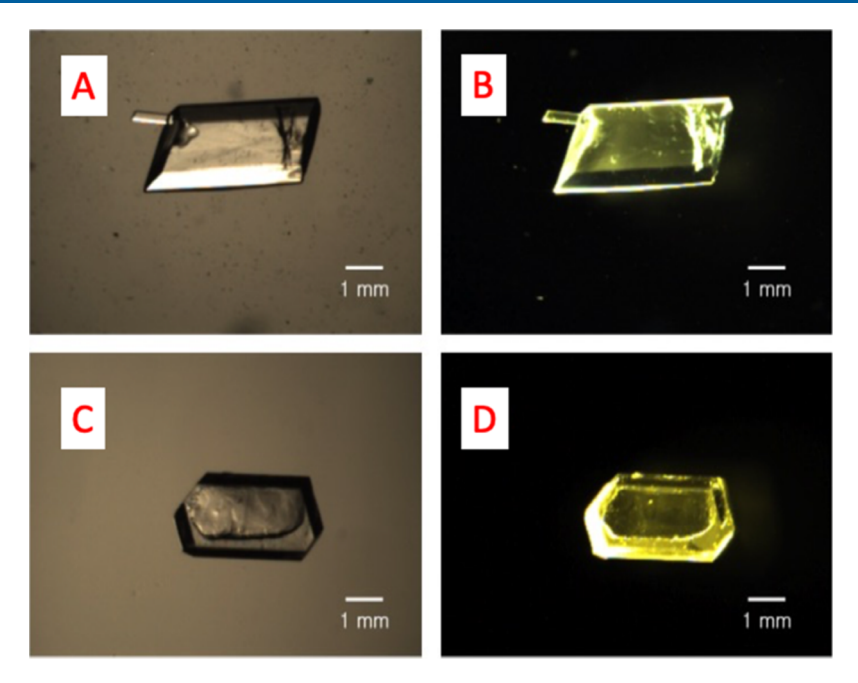


Figure 3. Photographs of crystals of  $\alpha$ -Au<sub>2</sub>( $\mu$ -dppe)<sub>2</sub>I<sub>2</sub>·2(HC(O)NMe<sub>2</sub>) (3) under (A) ambient light and (B) UV irradiation, and  $\beta$ -Au<sub>2</sub>( $\mu$ -dppe)<sub>2</sub>I<sub>2</sub>·2(HC(O)NMe<sub>2</sub>) (4) under (C) ambient light and (D) UV irradiation.

this system, are predominantly weak hydrogen-bonding interactions, namely, solvent—aryl-proton (2–20 kJ/mol) and proton-to-phenyl  $\pi$ -stacking (>3 kcal/mol). The <10 kJ/mol difference in energies between the two calculated structures and notable intermolecular forces in the packed structure strongly suggest that the differences in Au····Au distances in the two polymorphs are primarily a result of crystal packing effects resulting from the incorporation of various solvate molecules.

Another factor that affects the Au–Au separation is the relative orientations of the phenyl rings within  $\mathrm{Au_2}(\mu\text{-dppe})_2\mathrm{I_2}$ . The Supporting Information contains two animations that show the output from the relaxed surface scan where the Au···Au distance was surveyed from 4.599 to 2.959 Å over the course of 50 steps. The animation shows a glitch at about 65% through the animation or at an Au–Au separation of  $\sim$ 3.5 Å where the orientation of the phenyl rings changes from that shown in Figure 4B with pairs of phenyl rings nearly parallel to each other and an Au···Au separation of 3.7866(3) Å to that shown in Figure 4A, where the same pairs of phenyl rings are nearly perpendicular to one another and the Au····Au separationis 3.2366(3) Å.

Analysis of Au···Au Interactions. Single-point calculations on the three gold structures were used to determine the nature of the interactions between the two Au atoms in each structure using the calculated Mayer bond orders (MBO).<sup>20–22</sup> The Geom(Very\_Short) structure was calculated to have a Au–Au MBO of 0.11, indicating a weak but nonzero Au–Au bonding interaction. Both the Geom(Short) and Geom(Long) structures returned MBO values less than 0.10. Thus, Au–Au bonding interactions in these two structures are minimal. These bond order results agree with the comparison of the Au···Au distances to the sum of the Au van der Waals radii, described above.

Metal—metal bonding between the  $d^{10}$  Au(I) ions can occur at short Au—Au distances when the Au—Au antibonding highest filled molecular orbital (HFMO, consisting of an out-of-phase combination of 5d orbitals) is raised close enough in energy to mix significantly with the empty 6s and 6p orbitals. <sup>23–28</sup> This

mixing, particularly with the 6p orbitals, causes the HFMO to have nonbonding, rather than antibonding, character, as the orbital lobes bulge out away from the Au–Au centroid. The structures Geom(Very\_Short), Geom(Short), and Geom(Long) provide snapshots of this effect, which is seen via analysis of the orbital compositions given in Table 6 and Figure 6. Starting with Geom(Long), beyond the sum of the Au van der Waals radii, we see that the HFMO is essentially a hybrid of 5d and 6s orbitals with little 6p character (<3% of the metal contribution per Au atom). Geom(Short), which is very close to the sum of the Au van der Waals radii, has ~5% 6p character, while Geom(Very Short) has ~20% p character.

### CONCLUSIONS

Our results indicate that crystallization of materials containing the components Au<sup>+</sup>, dppe, and I<sup>-</sup> in a 1:1:1 ratio can produce solvates of the centrosymmetric dimer,  $Au_2(\mu$ -dppe)<sub>2</sub> $I_2$ , as well as the polymer,  $\{Au(\mu\text{-dppe})I\}_n \cdot n(CHCl_3)$  (6), and the iodide bridged dimer,  $Au_2(\mu\text{-dppe})_2(\mu\text{-I})_2$ , which was reported previously. 13 The centrosymmetric dimer,  $Au_2(\mu$ -dppe)  $_2I_2$ , is quite flexible with Au...Au separations that range from 3.192(1) to 3.7866(3) Å. However, none of the compounds we have isolated have Au...Au separations that are as short as 2.987 Å, the distance that was computed for the hypothetical Geom-(Very Short). Only the cationic dimer,  $[Au_2(\mu\text{-dppe})_2]^{2+}$ , with two-coordinate gold(I) ions has an Au···Au separation that short. 11,14 Thus, at short Au... Au contacts, the formation of the dimeric dication,  $[Au_2(\mu\text{-dppe})_2]^{2+}$ , with two-coordinate gold-(I) centers is preferable to retaining the iodide ligands to form the molecular dimer,  $Au_2(\mu$ -dppe)<sub>2</sub> $I_2$ , with three-coordinate gold(I) centers.

The pair of polymorphs of  $Au_2(\mu\text{-dppe})_2I_2\cdot 2(OC(CH_3)_2)$  were investigated computationally to better understand the origin of their different Au···Au distances. These two structures were computationally predicted to differ in energy by only  $\sim 10$  kJ/mol, an energy that is small enough to be attributable to crystal packing forces. An analysis of Au···Au interactions

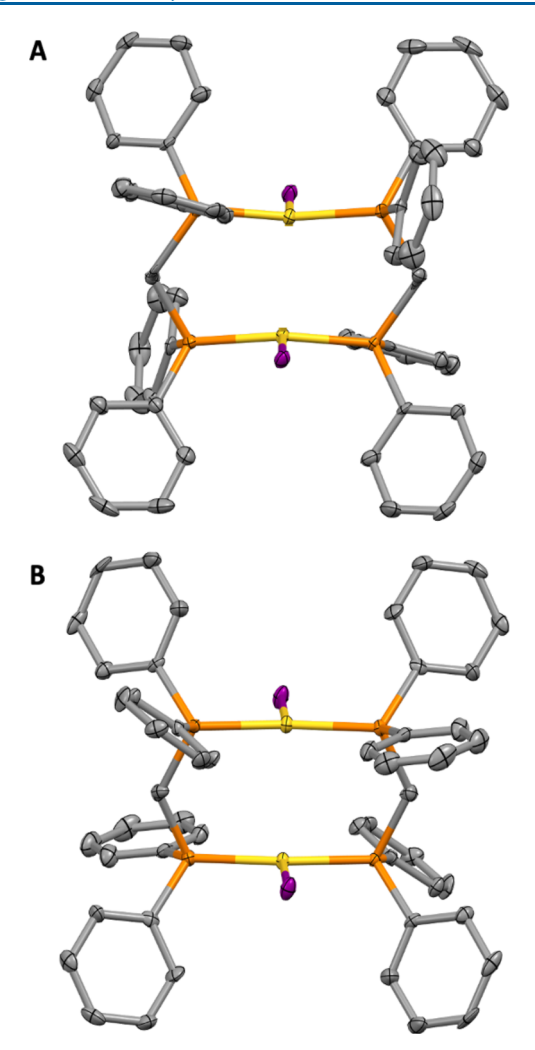


**Figure 4.** Structures of the two independent dimers in  $\beta$ -Au<sub>2</sub>( $\mu$ -dppe)<sub>2</sub>I<sub>2</sub>·2(HC(O)NMe<sub>2</sub>) (4) with the hydrogen atoms and solvate molecules removed for clarity. (A) Molecule with the shorter separation between the gold ions. (B) Molecule with the longer separation between the gold ions. Color code: gold, yellow; phosphorus, orange; iodine, purple; carbon, gray.

highlighted the changes in electronic structure that occurred as the Au atoms were brought together from a nonbonding range into the aurophilic bonding range. Notably, an increase in 6p contribution to the Au—Au highest filled metal orbital (HFMO) changes the nature of this orbital from Au—Au antibonding to

Au—Au nonbonding as the two Au atoms were brought together. However, this effect was minimal over the crystallographically observed Au···Au distances and only became relevant at a hypothetical Au—Au distance of <3.2 Å. Overall, the structural differences between the Au dimers were found to originate primarily from crystal packing effects with minimal aurophilic influence.

The interplay of coordination number and aurophilic interactions is not clear-cut. Two-coordinate gold(I) complexes frequently engage in aurophilic interactions, which are responsible for the self-association of some of these compounds. For three-coordinate gold(I), the issue is ambigous. As our computations have shown, aurophilic interactions are not significant at the distances found in our solvates of  $\mathrm{Au}_2(\mu\text{-dppe})_2\mathrm{I}_2$ . However, there are several three-coordinate gold(I) complexes involving  $\mathrm{AuP}_2\mathrm{I}$  coordination where shorter  $\mathrm{Au}$ ----Au distances may indicate aurophilic interactions. We have included relevant data about these complexes in Table 3. Finally, there are a least two cases of four-coordinate gold being involved in aurophilic interactions with other two-coordinate gold centers.  $^{29,30}$ 

The luminescence in the solvated crystals of  $\mathrm{Au}_2(\mu\text{-dppe})_2\mathrm{I}_2$  is associated with the presence of planar, three-coordinate gold centers, which are usually luminescent without the need for aurophilic interactions. The For such complexes, the excitation process generally involves a promotion of an electron from the doubly occupied, in-plane  $\mathrm{d}_{x^2-y^2}$ ,  $\mathrm{d}_{xy}$  gold orbitals into an empty orbital, which can be the out-of-plane  $p_x$  gold orbital or an empty ligand orbital. Specifically  $\mathrm{d}_{x^2-y^2}$ .

B3LYP density functional computations have been conducted on the related series of dimeric complexes,  $\operatorname{Au}_2(\mu-\operatorname{Ph}_2\operatorname{P-}(\operatorname{CH}_2)_n\operatorname{PPh}_2)_2\operatorname{I}_2$  (n=3-6), and on mononuclear Au-(PPh<sub>2</sub>Me)<sub>2</sub>I. Those calculations indicated that for compounds with an  $\operatorname{AuP}_2\operatorname{I}$  core, the excitation involves metal-to-ligand charge-transfer (MLCT) from an orbital with Au–I antibonding character to an orbital that is largely composed of phosphine ligand  $\pi$  bonds. These computations also examined variations in the P–Au–P bond angles and the Au–I distances and found a correlation between the Au–I distances in these complexes and the emission wavelength. That correlation is not observed in the crystals of  $\operatorname{Au}_2(\mu-\operatorname{dppe})_2\operatorname{I}_2$ , where the variation in emission wavelength is small as seen in Table 4.

## **■ EXPERIMENTAL SECTION**

Preparation of Au(dppe)I. A  $100 \, \mathrm{mg}$  (0.309 mmol) portion of AuI was suspended in  $30 \, \mathrm{mL}$  of dichloromethane and to this suspension was added  $185 \, \mathrm{mg}$  (0.463 mmol) of dppe. After stirring for  $3 \, \mathrm{h}$ , the

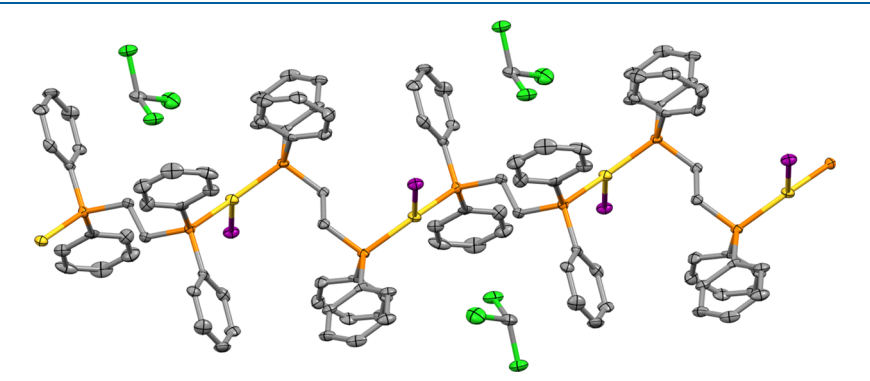


Figure 5. Structure of part of the polymeric chain in  $\{Au(\mu\text{-dppe})I\}_n \cdot n(CHCl_3)$  (6) with the hydrogen atoms removed for clarity. Color code: gold, yellow; phosphorus, orange; iodine, purple; carbon, gray; chlorine, green.

Table 5. Selected Geometric Features of  $Au_2(\mu\text{-dppe})_2I_2$  from the Experimental Crystal Structures and the Computed Systems

			Au-I				
	Au–Au, Å	Au-P Å	Au…I Å	I-Au-Au angle	P-Au-P angle	P-Au-I angle	origin
Geom(Short)	3.395 (fixed)	2.321	2.871 3.695	71.7°	146.0°	109.7° 104.3°	DFT
Au(Short)	3.3955(2)	2.316(2)	2.9759(2) 3.7143(2)	70.97(2)°	152.98(2)°	103.57(2)° 102.79(2)°	crystal ref 13
Geom(Long)	3.6720 (fixed)	2.321	2.871 3.842	70.7°	146.1°	108.8° 104.8°	DFT
Au(Long)	3.6720(2)	2.314(1)	2.9106(2) 3.937(2)	72.43(2)°	154.33(2)°	103.34(2)° 102.27(2)°	crystal ref 13
Geom(Very_Short)	2.987	2.327	2.865 3.576	75.3°	143.5°	111.5° 103.4°	DFT

Table 6. Percentage Contributions of Atomic Orbitals to the Filled Au—Au  $\sigma$  and  $\sigma^*$  Molecular Orbitals

	system	contributions (%)
Geom(Very_Short)		
highest occupied metal orbital	Au1	d: 9.4; s: 2.4; p: 2.9
	Au2	d: 9.4; s: 2.4; p: 2.9
	other	70.6
Geom(Short)		
highest occupied metal orbital	Au1	d: 8.8; s: 4.2; p: 0.7
	Au2	d: 8.8; s: 4.2; p: 0.7
	other	72.6
Geom(Long)		
highest occupied metal orbital	Au1	d: 4.8; s: 2.8; p: 0.2
	Au2	d: 4.8; s: 2.8; p: 0.2
	other	84.4

suspension became a clear solution. The solution was filtered, and then the solvent was removed in a vacuum. The white solid was collected and washed with diethyl ether: yield, 195 mg (87.4%). This material was used to obtain crystalline samples of the following compounds.

 $Au_2(\mu\text{-dppe})_2l_2\cdot 4(CH_2Cl_2)$  (1). Crystals suitable for X-ray structure determination were grown by slow diffusion of diethyl ether to a solution of the colorless solid in chloroform. Colorless, block-shaped crystals with yellow luminescence grew in the mixture in about 3 to 4 days.

Infrared spectrum: 3035w, 2933m, 2920m, 2849m, 1718w, 1441w, 1431s, 1433w, 1430w, 1377w, 1274m, 1177m, 1174m, 1096m, 1098m, 1027m, 999m, 995m, 727s, 699s cm $^{-1}$ .

 $Au_2(\mu\text{-}dppe)_2l_2\cdot 2(CH_2Cl_2)$  (2). The suitable crystals for X-ray structure determination were grown by slow diffusion of diethyl ether to a saturated solution of the initial white solid in dichloromethane. The colorless blocks of  $Au_2(\mu\text{-}dppe)_2I_2\cdot 2(CH_2Cl_2)$  with a yellow luminescence formed over a 2- to 3-day period.

Infrared spectrum: 3048w, 2891w, 1480s, 1434m, 1415m, 1305w, 1264w, 1156w, 1098s, 1069m, 998w, 820m, 741m, 727m, 705m, 689s, 521m, 508s, 486m cm $^{-1}$ 

 $\alpha$ -Au<sub>2</sub>( $\mu$ -dppe)<sub>2</sub>l<sub>2</sub>·2(HC(O)NMe<sub>2</sub>) (3) and  $\beta$ -Au<sub>2</sub>( $\mu$ -dppe)<sub>2</sub>l<sub>2</sub>·2(HC-(O)NMe<sub>2</sub>) (4). The white solid was dissolved in a minimum volume of N,N-dimethylformamide, and the colorless solution was filtered. After evaporation for a week, two different kinds of colorless blocks grew in the solution. These crystals, which produced yellow-green and yellow-orange luminescence, respectively, were separated manually and used for spectroscopy and crystallography.

Infrared spectrum green emissive  $\alpha$ -Au<sub>2</sub>( $\mu$ -dppe)<sub>2</sub>I<sub>2</sub>·2(HC(O)-NMe<sub>2</sub>) (3): 3053w, 2927w, 2893w, 1660s( $\nu$  C=O from HC(O)-NMe<sub>2</sub>), 1483m, 1433m, 1386m, 1098s, 1053m, 1024m, 952m, 822m, 741m, 721m, 705m, 688s, 659m, 519m, 507s, 488m, 478m cm<sup>-1</sup>

Infrared spectrum yellow emissive  $\beta$ -Au<sub>2</sub>( $\mu$ -dppe)<sub>2</sub>I<sub>2</sub>·2(HC(O)-NMe<sub>2</sub>) (4): 3054w, 2929w, 2894w, 1662s( $\nu$  C=O from HC(O)-NMe<sub>2</sub>), 1483m, 1434m, 1414m, 1385m, 1097s, 1053m, 1023m, 951m, 822m, 742m, 721m, 705m, 688s, 659m,519m, 508s, 486m, 478m cm<sup>-1</sup>

 $Au_2(\mu\text{-dppe})_2l_2\cdot 4(CHCl_3)$  (5). Crystals suitable for X-ray structure determination were grown by slow diffusion of diethyl ether to a solution of the colorless solid in chloroform. Colorless, block-shaped crystals of  $Au_2(\mu\text{-dppe})_2l_2\cdot 4(CHCl_3)$  (5) appeared within 2 to 3 days.

Infrared spectrum: 2940m, 2922vs, 2852m, 2362w, 2332w, 1464m, 1435w, 1377w, 1260w, 1187w, 1171w, 1175m, 1099m,1072w, 1027w, 998w, 802w, 740s, 728s, 691vs cm<sup>-1</sup>

Polymeric  $\{Au(\mu\text{-}dppe)l\}_n\cdot n(CHCl_3)$  (6). Crystals suitable for X-ray structure determination were grown by slow diffusion of diethyl ether to a solution of the colorless solid in chloroform. Colorless, irregular plates of  $\{Au(\mu\text{-}dppe)l\}_n\cdot n(CHCl_3)$  (6) appeared in 3 to 4 days.

Infrared spectrum: 3049w, 2975w, 2899w, 1481s, 1433s, 1412m, 1315m, 1099s, 1072m, 950m, 750m, 726s, 692s, 521m, 509s, 486m, 477m

X-ray Crystallography and Data Collection. The crystals were removed from the glass tubes in which they were grown together with a small amount of mother liquor and immediately coated with a hydrocarbon oil on a microscope slide. A suitable crystal of each compound was mounted on a glass fiber with silicone grease and placed in the liquid nitrogen cold stream of a Bruker SMART CCD with graphite monochromated Mo K $\alpha$  radiation at 90(2) K. Check reflections were stable throughout the data collection.

The structures were solved by direct methods and refined using all data (based on  $F^2$ ) using the software SHELXTL 5.1. A semiempirical



Figure 6. Isosurface plots (at 50%) of the highest filled metal orbitals for Geom(Very\_Short), Geom(Short), and Geom(Long), highlighting the increasing degree of Au—Au antibonding character across the series.

method utilizing equivalents was employed to correct for absorptions. Hydrogen atoms were added geometrically and refined with a riding model.  $^{35}$ 

**Physical Measurements.** Infrared spectra were recorded on a Bruker  $\alpha$  Fourier transform infrared (FT-IR) spectrometer. Fluorescence excitation and emission spectra were recorded on a PerkinElmer LS50B luminescence spectrophotometer.

Computational Methods. Geometry optimizations, frequency calculations, and single-point (SP) were carried out using ORCA version 5.0.1.36,37 For the geometry optimizations and frequency calculations, the BP86 exchange-correlation functional was used.<sup>38</sup> Crystallographic coordinates, excluding solvent molecules, were used as the starting point for all geometry optimizations. The two experimental crystal structures were used as a basis for two computational models, Geom(Short) and Geom(Long), having Au···Au distances fixed to those of the two polymorphs. 13 All other geometric parameters were optimized. A third model, Geom(Very Short), with an even shorter Au-Au distance of 2.99 Å, resulted from a full geometry optimization without fixing the Au···Au distances. All calculations used the resolution of identity and correlation of spheres, RIJCOSX approximation.<sup>4</sup> The segmented all-electron relativistic contracted (SARC) basis set, SARC-DKH-TZVPP, 45-47 was used for the Au atoms. The SARC contracted Karlsruhe basis set, SARC-DKH-TZVP, 48 was used for I atoms, while def2-SVP<sup>49</sup> was used for all other atoms. The auxiliary coulomb basis set, def2/J,50 was used for all atoms. Dispersion corrections to the calculations were accounted for with the atom pairwise dispersion correction employing the Becke-Johnson damping scheme (D3BJ). 51,52 All molecules were calculated in their open-shell singlet state using unrestricted Kohn-Sham (UKS) theory. The radial grid of the Au atoms was set to 10, whereas the grids for all other atoms were set to 6. Frequency calculations were performed by numerical differentiation with a central-differences increment of 0.01. Visualizations of the orbitals from self-consistent field calculations were carried out with the UCSF Chimera package. 53 Structure comparisons were made using Mercury.54

### ASSOCIATED CONTENT

### Supporting Information

The Supporting Information is available free of charge at https://pubs.acs.org/doi/10.1021/acs.inorgchem.4c00783.

Drawings of the molecular structures of compounds (1), (2), (3), and (5). Cartesian coordinates from geometry optimizations (PDF)

This short animation displays the output from the relaxed surface scan where the Au–Au distance was surveyed from 4.599 to 2.959 Å over the course of 50 steps (BP86 Side) (MPG)

This short animation displays the output from the relaxed surface scan where the Au—Au distance was surveyed from 4.599 to 2.959 Å over the course of 50 steps (BP86) (MPG)

## **Accession Codes**

CCDC 2334751—2334756 contain the supplementary crystallographic data for this paper. These data can be obtained free of charge via <a href="www.ccdc.cam.ac.uk/data\_request/cif">www.ccdc.cam.ac.uk/data\_request/cif</a>, by emailing <a href="mailto:data\_request@ccdc.cam.ac.uk">data\_request@ccdc.cam.ac.uk</a>, or by contacting The Cambridge Crystallographic Data Centre, 12 Union Road, Cambridge CB2 1EZ, U.K.; fax: +44 1223 336033.

## AUTHOR INFORMATION

#### **Corresponding Authors**

John F. Berry — Department of Chemistry, University of Wisconsin-Madison, Madison, Wisconsin 53706, United States; orcid.org/0000-0002-6805-0640; Email: berry@chem.wisc.edu

Alan L. Balch — Department of Chemistry, University of California-Davis, Davis, California 95616, United States; orcid.org/0000-0002-8813-6281; Email: albalch@ucdavis.edu

#### **Authors**

Sarah Costa — Department of Chemistry, University of California-Davis, Davis, California 95616, United States Michael M. Aristov — Department of Chemistry, University of Wisconsin-Madison, Madison, Wisconsin 53706, United States Sang Ho Lim — Nuclear Chemistry Technology Division, Korea Atomic Energy Research Institute, Daejeon 34057, Republic of Korea; Orcid.org/0000-0002-8583-5677

Sarah M. Chui — Department of Chemistry, University of California-Davis, Davis, California 95616, United States

Katelyn A. Espinoza — Department of Chemistry, University of California-Davis, Davis, California 95616, United States

Marilyn M. Olmstead — Department of Chemistry, University of California-Davis, Davis, California 95616, United States;

orcid.org/0000-0002-6160-1622

James C. Fettinger — Department of Chemistry, University of California-Davis, Davis, California 95616, United States;
orcid.org/0000-0002-6428-4909

Complete contact information is available at: https://pubs.acs.org/10.1021/acs.inorgchem.4c00783

#### **Notes**

The authors declare no competing financial interest. Deceased, Sept. 30, 2020.

## ACKNOWLEDGMENTS

The authors thank the Petroleum Research Fund (Grant 37056-AC to A.L.B.) and U.S. National Science Foundation [CHE-0716843 and CHE-1807637 to A.L.B. and M.M.O.; CHE-2246913 to J.F.B.] for support.

## REFERENCES

- (1) Paderina, A. V.; Koshevoy, I. O.; Grachova, E. V. Keep it tight: a crucial role of bridging phosphine ligands in the design and optical properties of multinuclear coinage metal complexes. *Dalton Trans.* **2021**, *50*, 6003–6033.
- (2) Puddephatt, R. J. Macrocycles, catenanes, oligomers and polymers in gold chemistry. *Chem. Soc. Rev.* **2008**, *37*, 2012–2027.
- (3) Puddephatt, R. J. Chemistry of Bis(diphenylphosphino)methane. *Chem. Soc. Rev.* **1983**, *12*, 99–127.
- (4) Chaudret, B.; Delavaux, B.; Poilblanc, R. Bisdiphenylphosphinomethane in Dinuclear Complexes. *Coord. Chem. Rev.* **1988**, *86*, 191–242
- (5) Balch, A. L.; Tulyathan, B. Interactions between Rhodium(I) Centers in Dimeric Complexes. *Inorg. Chem.* **1977**, *16*, 2840–2845.
- (6) Haddow, M. F.; Middleton, A. J.; Orpen, A. G.; Pringle, P. G.; Papp, R. Stereoelectronic effects in a homologous series of bidentate cyclic phosphines. A clear correlation of hydroformylation catalyst activity with ring size. *Dalton Trans.* **2009**, 202–209.
- (7) Lim, S. H.; Schmitt, J. C.; Shearer, J.; Jia, J.; Olmstead, M. M.; Fettinger, J. C.; Balch, A. L. Crystallographic and Computational Studies of Luminescent, Binuclear Gold(I) Complexes,  $Au_2^{\ I}(Ph_2P-(CH_2)_nPPh_2)_2I_2$  (n = 3-6). *Inorg. Chem.* **2013**, *52*, 823-831.
- (8) Streitberger, M.; Schmied, A.; Hey-Hawkins, E. Selective Formation of Gold(I) Bis-Phospholane Macrocycles, Polymeric Chains, and Nanotubes. *Inorg. Chem.* **2014**, *53*, 6794–6804.
- (9) Boar, P.; Lönnecke, P.; Hey-Hawkins, E. Silver(I) Complexes of Two Flexible Bis-phospholane Ligands: Metallamacrocycles, Polymeric Chains, and Metallacryptands. *Z. Anorg. Allg. Chem.* **2020**, *646*, 915–922.

- (10) Boar, P.; Streitberger, M.; Lönnecke, P.; Hey-Hawkins, E. Copper(I) Complexes of a Flexible Bis-phospholane Ligand: Route to Paddle-Wheel- and Box-Type Macrocycles. *Inorg. Chem.* **2017**, *56*, 7285–7291.
- (11) Costa, S.; Walters, D. T.; McNamara, L. E.; Olmstead, M. M.; Fettinger, J. C.; Balch, A. L. Structure and Luminescence Studies of Salts of the Helical Dication,  $[Au_2(\mu\text{-bis}(\text{diphenylphosphine})\text{-ethane})_2]^{2+}$  and Comparison with Salts of  $[Au_2(\mu\text{-bis}(\text{diphenylphosphine})\text{-propane})_2]^{2+}$ . *Inorg. Chem.* **2023**, *62*, 15902–15911.
- (12) Lim, S. H.; Olmstead, M. M.; Balch, A. L. Molecular Accordion: Vapoluminescence and Molecular Flexibility in the Orange and Green Luminescent Crystals of the Dimer,  $Au_2(\mu$ -bis-(diphenylphosphino)-ethane)<sub>2</sub>Br<sub>2</sub>. *J. Am. Chem. Soc.* **2011**, *133*, 10229–10238.
- (13) Lim, S. H.; Olmstead, M. M.; Balch, A. L. Inorganic topochemistry. Vapor-induced solid state transformations of luminescent, three-coordinate gold(I) complexes. *Chem. Sci.* **2013**, *4*, 311–318.
- (14) Schuh, W.; Kopacka, H.; Wurst, K.; Peringer, P. Observation of a P/M interconversion of a gold–phosphine helicate via <sup>31</sup>P NMR. *Chem. Commun.* **2001**, 2186–2187.
- (15) Schmidbaur, H.; Schier, A. Aurophilic Interactions In and Between Molecules as a Subject of Current Interest. *Chem. Soc. Rev.* **2012**, *41*, 370–412.
- (16) Mirzadeh, N.; Privér, S. H.; Blake, A. J.; Schmidbaur, H.; Bhargava, S. K. Innovative Molecular Design Strategies in Materials Science Following the Aurophilicity Concept. *Chem. Rev.* **2020**, *120*, 7551–7591.
- (17) Balch, A. L. Polymorphism and Luminescent Behavior of Linear, Two-Coordinate Gold(I) Complexes. *Gold Bull.* **2004**, *37*, 45–50.
- (18) England, K. R.; Lim, S. H.; Luong, L. M. C.; Olmstead, M. M.; Balch, A. L. Vapoluminescent Behavior and the Single-Crystal-to Single-Crystal Transformations of Chloroform Solvates of  $[Au_2(\mu-1,2-bis(diphenylarsino)ethane)_2](AsF_6)_2$ . Chem. Eur. J. **2019**, 25, 874–878.
- (19) Luong, L. M. C.; Lowe, C. D.; Adams, A. V.; Moshayedi, V.; Olmstead, M. M.; Balch, A. L. Seeing luminescence appear as crystals crumble. Isolation and subsequent self-association of individual  $[(C_6H_{11}NC)_2Au]^+$  ions in crystals. *Chem. Sci.* **2020**, *11*, 11705–11713.
- (20) Bridgeman, A. J.; Cavigliasso, G.; Ireland, L. R.; Rothery, J. The Mayer bond order as a tool in inorganic chemistry. *Dalton Trans.* **2001**, *14*, 2095–2108.
- (21) Mayer, I. Charge, bond order and valence in the AB initio SCF theory. Chem. Phys. Lett. 1983, 97 (3), 270–274.
- (22) Mayer, I. Bond order and valence: Relations to Mulliken's population analysis. *Int. J. Quantum Chem.* **1984**, 26 (1), 151–154.
- (23) Pyykkö, P. Relativistic Quantum Chemistry. In Advances in Quantum Chemistry; Elsevier, 1978; Vol. 11, pp 353-409.
- (24) Pyykko, P.; Desclaux, J. P. Relativity and the periodic system of elements. Acc. Chem. Res. 1979, 12 (8), 276–281.
- (25) Pyykkö, P. Strong closed-shell interactions in inorganic chemistry. *Chem. Rev.* **1997**, *97*, 597–636.
- (26) Schmidbaur, H. The aurophilicity phenomenon: a decade of experimental findings, theoretical concepts and emerging applications. *Gold Bull.* **2000**, 33, 3–10.
- (27) Hutchings, G. J.; Brust, M.; Schmidbaur, H. Gold—an introductory perspective. *Chem. Soc. Rev.* **2008**, *37*, 1759–1765.
- (28) Wang, S.-G.; Schwarz, W. H. E. Quasi-Relativistic Density Functional Study of Aurophilic Interactions. *J. Am. Chem. Soc.* **2004**, 126, 1266–1276.
- (29) Schmidbaur, H.; Hartmann, C.; Reber, G.; Muller, G. Isovalent and Mixed-Valent Ylide Complexes of Gold: The Synthesis of Trinuclear Compounds Having Double Paddlewheel Structure. *Angew. Chem., Int. Ed.* **1987**, *26*, 1146–1148.
- (30) Zank, J.; Schier, A.; Schmidbaur, H. Gold and silver cations in the "Procrustean Bed" of the bis[2-(diphenylphosphino)phenyl]-phenylphosphine ligand. Observations and conclusions. *J. Chem. Soc., Dalton Trans.* 1999, 415–420.
- (31) Ziolo, R. F.; Lipton, S.; Z Dori, Z. The Photoluminescence of Phosphine Complexes of *d*<sup>10</sup> Metals. *J. Chem. Soc. D* **1970**, 1124–1125.

- (32) King, C.; Khan, M. N. I.; Staples, R. J.; Fackler, J. P., Jr. Luminescent mononuclear gold(I) phosphines. *Inorg. Chem.* **1992**, *31*, 3236–3238.
- (33) Barakat, K. A.; Cundari, T. R.; Omary, M. A. Jahn-Teller Distortion in the Phosphorescent Excited State of Three-Coordinate Au(I) Phosphine Complexes. *J. Am. Chem. Soc.* **2003**, *125*, 14228–14229
- (34) Sinha, P.; Wilson, A. K.; Omary, M. A. Beyond a T-Shape. *J. Am. Chem. Soc.* **2005**, *127*, 12488–12489.
- (35) Sheldrick, G. M. A short history of SHELX. Acta Crystallogr., Sect. A: Found. Crystallogr. 2008, 64, 112–122.
- (36) Neese, F. The ORCA program system. WIREs Comput. Mol. Sci. 2012, 2, 73–78.
- (37) Neese, F. Software update: The ORCA program system—Version 5.0. WIREs Comput. Mol. Sci. 2022, 12, No. e1606.
- (38) Becke, A. D. Density-functional exchange-energy approximation with correct asymptotic behavior. *Phys. Rev. A* **1988**, *38*, No. 3098, DOI: 10.1103/PhysRevA.38.3098.
- (39) Stephens, P. J.; Devlin, F. J.; Chabalowski, C. F.; Frisch, M. J. Ab initio calculation of vibrational absorption and circular dichroism spectra using density functional force fields. *J. Phys. Chem. A* **1994**, 98 (45), 11623–11627.
- (40) Becke, A. D. Density-functional thermochemistry. III. The role of exact exchange. *J. Chem. Phys.* **1993**, *98*, 5648–5652.
- (41) Lee, C.; Yang, W.; Parr, R. G. Development of the Colle-Salvetti correlation-energy formula into a functional of the electron density. *Phys. Rev. B* **1988**, *37*, No. 785, DOI: 10.1103/PhysRevB.37.785.
- (42) Guevara-Vela, J. M.; Rocha-Rinza, T.; Pendás, Á. M. Performance of the RI and RIJCOSX approximations in the topological analysis of the electron density. *Theor. Chem. Acc.* **2017**, *136*, No. 57, DOI: 10.1007/s00214-017-2084-0.
- (43) Neese, F. An improvement of the resolution of the identity approximation for the formation of the Coulomb matrix. *J. Comput. Chem.* **2003**, *24*, 1740–1747.
- (44) Neese, F.; Wennmohs, F.; Hansen, A.; Becker, U. Efficient, approximate and parallel Hartree—Fock and hybrid DFT calculations. A 'chain-of-spheres' algorithm for the Hartree—Fock exchange. *Chem. Phys.* **2009**, 356, 98–109.
- (45) Weigend, F. Accurate Coulomb-Fitting Basis Sets for H to Rn. *Phys. Chem. Chem. Phys.* **2006**, *8*, 1057–1065.
- (46) Pantazis, D. A.; Chen, X.-Y.; Landis, C. R.; Neese, F. All-Electron Scalar Relativistic Basis Sets for Third-Row Transition Metal Atoms. *J. Chem. Theory Comput.* **2008**, *4*, 908–919.
- (47) Peterson, K. A.; Puzzarini, C. Systematically Convergent Basis Sets for Transition Metals. II Pseudopotential-Based Correlation Consistent Basis Sets for the Group 11 (Cu, Ag, Au) and 12 (Zn, Cd, Hg) Elements. *Theor. Chem. Acc.* 2005, 114, 283–296.
- (48) Rolfes, J. D.; Neese, F.; Pantazis, D. A. All-electron scalar relativistic basis sets for the elements Rb—Xe. *J. Comput. Chem.* **2020**, *41*, 1842—1849.
- (49) Weigend, F.; Ahlrichs, R. Balanced Basis Sets of Split Valence, Triple Zeta Valence and Quadruple Zeta Valence Quality hor H To Rn: Design and Assessment of Accuracy. *Phys. Chem. Chem. Phys.* **2005**, *7*, 3297–3305.
- (50) Weigend, F. Accurate Coulomb-fitting basis sets for H to Rn. *Phys. Chem. Chem. Phys.* **2006**, *8*, 1057–1065.
- (51) Grimme, S.; Antony, J.; Ehrlich, S.; Krieg, H. A Consistent and Accurate ab initio Parametrization of Density Functional Dispersion Correction (DFT-D) for the 94 Elements H-Pu. *J. Chem. Phys.* **2010**, 132, No. 154104.
- (52) Grimme, S.; Ehrlich, S.; Goerigk, L. Effect of the Damping Function in Dispersion Corrected Density Functional Theory. *J. Comput. Chem.* **2011**, 32, 1456–1465.
- (53) Pettersen, E. F.; Goddard, T. D.; Huang, C. C.; Couch, G. S.; Greenblatt, D. M.; Meng, E. C.; Ferrin, T. E. UCSF Chimera—A Visualization System for Exploratory Research and Analysis. *J. Comput. Chem.* **2004**, *25*, 1605–1612.
- (54) Macrae, C. F.; Sovago, I.; Cottrell, S. J.; Galek, P. T. A.; McCabe, P.; Pidcock, E.; Platings, M.; Shields, G. P.; Stevens, J. S.; Towler, M.;

Wood, P. A. Mercury 4.0: from visualization to analysis, design and prediction. *J. Appl. Crystallogr.* **2020**, 53, 226–235.